Impaired Control of IRES-Mediated Translation in X-Linked Dyskeratosis Congenita

Andrew Yoon, *et al.*

Science **312**, 902 (2006);
DOI: 10.1126/science.1123835

is consistent with Korte and Constable's low-resolution geomagnetic field model CALS7K.2 (*6*, *7*), which has a slower decay of the dipole moment from 1600 to 1800 A.D. compared with that from 1800 to 1950 A.D. Their model, which spans the interval 5000 B.C. to 1950 A.D., was constructed from paleointensity and paleodirection data only (*2*, *6*) and therefore lacks information from the vastly more accurate historical measurements included in the present study.

What changed to precipitate the present fall in dipole moment? More insight comes from directional data, which are excellent from 1700 A.D. and suggest a change occurring around 1800 A.D. The geomagnetic field originates in the liquid core, and its dipole moment may be written as an average of the magnetic field at the core surface

$$g_1^0 = \frac{3c}{8\pi a^3}\int_S Z\cos\theta dS \qquad (1)$$

where Z is the downward component of magnetic field; θ is colatitude; a and c are Earth and core radii, respectively; and the integral is taken over the surface S of the liquid core. The source of any change in dipole moment can therefore be found from the change in $Z\cos\theta$ on the core surface, which comes mostly from growth and southward migration of patches of reversed flux in the Southern Hemisphere (Fig. 4). No intensity information is required to identify these reverse-flux patches; they are imaged well by the early directional data. One distinct patch first appeared in about 1780 A.D. (*8*) and continues to grow and drift south today (*8*, *9*).

An equal-area plot of $\dot{Z}\cos\theta$ reveals the regions on the core surface responsible for the fall (Fig. 5). The interval 1840 to 1980 (Fig. 5A) is dominated by the blue patch between Antarctica and the tip of South America, with additional contributions from other blue patches in the Southern Hemisphere. Orange and blue patches in the Northern Hemisphere are of similar size and cancel out. The separate contributions of the two hemispheres to the change in g_1^0 is $(\dot{g}_N, \dot{g}_S, \dot{g}_1^0) = (-0.1, 16.2, 16.1)$ nT/year, showing that almost all of the dipole decay has come from the Southern Hemisphere.

The interval 1590 to 1840 A.D. (Fig. 5B), which uses the mean fall in g_1^0 of 2.28 nT/year obtained in this study, shows much smaller amplitudes, and the patch between Antarctica and South America is almost balanced by the patches of opposite sign to the west, indicating longitudinal drift rather than southward movement or growth. The separate contributions of the integral for this interval are $(\dot{g}_N, \dot{g}_S, \dot{g}_1^0) = (-0.8, 3.1, 2.3)$; the Northern Hemisphere value is again effectively zero, but the Southern Hemisphere value is much lower than in the 19th and 20th centuries. This is consistent with a change in Southern Hemisphere behavior starting around 1800 A.D.; before that date the two hemispheres behaved in a similar manner.

Paleomagnetic data from the past 2500 years suggest a 40% fall in moment (*6*, *10*), or 1.6% per century. This is smaller than the present fall (5% per century) and is consistent with periods of rapid fall, as at present, interspersed with periods of little or no activity, as during 1590 to 1840 A.D. Patches of reverse flux almost certainly arise from expulsion of toroidal flux (*11*), and our present result suggests a quiet period up to 1800 when toroidal flux was brought up close to the core surface followed by active periods of expulsion through the core surface. The challenge now is to understand the magnetohydrodynamics of how such behavior can come about and to discover similar, earlier intervals of dipole decay interspersed with quiescence in the paleomagnetic record.

References and Notes

1. A. Jackson, A. R. T. Jonkers, M. R. Walker, *Philos. Trans. R. Soc. London A* **358**, 957 (2000).
2. M. Korte, A. Genevey, C. G. Constable, U. Frank, E. Schnepp, *Geochem. Geophys. Geosyst.* 10.1029/2004GC000800 (1 February 2005).
3. G. Hulot, A. Khokhlov, J. L. LeMouel, *Geophys. J. Int.* **129**, 347 (1997).
4. J. H. Williamson, *Can. J. Phys.* **46**, 1846 (1968).
5. W. H. Press, B. P. Flannery, S. A. Teukolsky, W. T. Vetterling, *Numerical Recipes in FORTRAN* (Cambridge Univ. Press, Cambridge, UK, 2002).
6. M. Korte, C. G. Constable, *Geochem. Geophys. Geosyst.* 10.1029/2004GC000801 (1 February 2005).
7. M. Korte, C. G. Constable, *Earth Planet. Sci. Lett.* **236**, 348 (2005).
8. J. Bloxham, D. Gubbins, A. Jackson, *Philos. Trans. R. Soc. London* **329**, 415 (1989).
9. G. Hulot, C. Eymin, B. Langlais, M. Mandea, N. Olsen, *Nature* **416**, 620 (2002).
10. M. W. McElhinny, W. E. Senanayake, *J. Geomagn. Geoelectr.* **34**, 39 (1980).
11. D. Gubbins, *Phys. Earth Planet. Int.* **98**, 193 (1996).

12. This work formed part of A.L.J.'s undergraduate project, which was supported by a Local Education Authority grant. C.C.F. was supported by a Ph.D. studentship from the Natural Environment Research Council (NER/S/A/2001/06265).

11 January 2006; accepted 14 March 2006
10.1126/science.1124855

Impaired Control of IRES-Mediated Translation in X-Linked Dyskeratosis Congenita

Andrew Yoon,[1]* Guang Peng,[1]* Yves Brandenburg,[1]* Ornella Zollo,[1] Wei Xu,[1] Eduardo Rego,[2] Davide Ruggero[1]†

The *DKC1* gene encodes a pseudouridine synthase that modifies ribosomal RNA (rRNA). *DKC1* is mutated in people with X-linked dyskeratosis congenita (X-DC), a disease characterized by bone marrow failure, skin abnormalities, and increased susceptibility to cancer. How alterations in ribosome modification might lead to cancer and other features of the disease remains unknown. Using an unbiased proteomics strategy, we discovered a specific defect in IRES (internal ribosome entry site)–dependent translation in *Dkc1*^{m} mice and in cells from X-DC patients. This defect results in impaired translation of messenger RNAs containing IRES elements, including those encoding the tumor suppressor p27(Kip1) and the antiapoptotic factors Bcl-xL and XIAP (X-linked Inhibitor of Apoptosis Protein). Moreover, *Dkc1*^{m} ribosomes were unable to direct translation from IRES elements present in viral messenger RNAs. These findings reveal a potential mechanism by which defective ribosome activity leads to disease and cancer.

X-linked dyskeratosis congenita (X-DC) is a rare and often fatal disease characterized by multiple pathological features, including bone marrow failure and increased susceptibility to cancer (*1*). X-DC is caused by mutations in the *DKC1* gene that encodes dyskerin, a protein associated with small RNAs that share the H+ACA RNA motif, including the telomerase RNA (TR), Cajal body RNAs (scaRNAs), and small nucleolar RNAs (snoRNAs) (*2*). When associated with snoRNAs, dyskerin acts as a pseudouridine synthase to mediate posttranscriptional modification of ribosomal RNA (rRNA) through the conversion of uridine (U) to pseudouridine (Ψ) (*3*, *4*). X-DC patient cell lines and mouse embryonic stem cells harboring knocked-in *DKC1* point mutations exhibit reduced rRNA pseudouridylation (*2*, *5*). Hypomorphic *Dkc1*^{m} mice recapitulate many of the clinical features of X-DC and display reductions in rRNA modification, suggesting that impairments in ribosome function may have a causative effect on X-DC pathogenesis (*6*). However, the role of rRNA modifications in the control of protein synthesis remains poorly understood. In addition, how alterations in the translational apparatus could lead to specific pathological features associated with human disease remains unknown. We investigated the role of rRNA modifications in the control of protein synthesis in order to understand the molecular basis of X-DC.

[1]Human Genetics Program, Fox Chase Cancer Center, Philadelphia, PA 19111, USA. [2]Center for Cell Based Therapy, Fundação Hemocentro de Ribeirão Preto, University of Sao Paulo, Brazil.

*These authors contributed equally to this work.
†To whom correspondence should be addressed. E-mail: davide.ruggero@fccc.edu

We first determined whether decreased rRNA pseudouridylation results in impaired general (cap-dependent) translation, using *Dkc1*^{m} mice. Total protein synthesis rates were no different in primary *Dkc1*^{m} cells than in wild-type cells (fig. S1), and therefore decreased rRNA pseudouridylation in *Dkc1*^{m} ribosomes does not impair general protein synthesis. We next hypothesized that the reduction of modified uridine residues in *Dkc1*^{m} ribosomes might affect the translation of specific mRNAs and hence may not be readily evident when monitoring for general cap-dependent protein synthesis. We therefore established an unbiased proteomics protocol to screen for candidate mRNAs that rely on *Dkc1*-dependent rRNA modifications for efficient protein translation. In particular, we optimized a glycerol gradient (*7*) to purify mRNAs associated with translationally active ribosomes (polysomes) from steady-state and activated primary splenic lymphocytes, one of the hematopoietic lineages affected in X-DC (Fig. 1A). Purified polysome-associated mRNAs from wild-type and *Dkc1*^{m} lymphocytes, before disease onset, were used to hybridize two commercially available mouse cDNA microarrays (*7*). These microarrays contained in total 1500 spotted cDNAs with a wide variety of biological functions, including cell signaling, cell differentiation, control of the cell cycle and apoptosis, or genes implicated in cancer initiation (*8*–*10*). Using this protocol, we identified 3 out of 1500 mRNAs that were specifically decreased in polysome association in *Dkc1*^{m} lymphocytes. In particular, the p27 tumor suppressor and the antiapoptotic proteins XIAP (X-linked Inhibitor of Apoptosis Protein) and Bcl-xL showed a significant decrease (25% or greater) in their association with polysomes in *Dkc1*^{m} cells as compared to wild-type cells. To validate the microarray results, translational control of p27, XIAP, and Bcl-xL mRNAs was monitored in *Dkc1*^{m} cells (Fig. 1, B and C). Protein levels of these target mRNAs were significantly down-regulated in *Dkc1*^{m} lymphocytes (Fig. 1, B and C), whereas no differences were apparent in mRNA transcript levels or protein stability (figs. S2 and S3). In addition, mRNAs showing less than a 25% decrease in polysome association did not reveal differences in gene expression (fig. S2). Altogether, these data reveal defects in the translation of specific mRNAs in *Dkc1*^{m} cells.

Having determined that general protein synthesis is unaffected in *Dkc1*^{m} cells, we hypothesized that a cap-independent mechanism relying on dyskerin activity may account for differences in the translation of these mRNAs. Two of the mRNAs identified in our screen, p27(Kip1) and XIAP, share a common feature in their mode of translation initiation, because they both harbor an internal ribosome entry site (IRES) element, previously shown to be important for their accurate expression (*11*–*13*). IRES elements, which are present within a subset of cellular mRNAs, are structured RNAs of variable length that bind the ribosome during translation initiation, thereby bypassing the requirement for some of the cap-binding proteins (*14*). Although IRES elements are active in normal growth conditions, IRES-dependent translation is favored during specific cellular stimuli such as the induction of programmed cell death or during distinct phases of the cell cycle, when cap-dependent translation is decreased (*15*). We therefore tested whether decreased XIAP and p27 protein expression in *Dkc1*^{m} cells was due to a defect in IRES-dependent translation. We initially analyzed endogenous levels of XIAP and p27 proteins under conditions in which IRES-mediated translation is stimulated, using mouse embryonic fibroblasts (MEFs). We examined XIAP protein levels when the MEFs were exposed to γ irradiation, a stimulus that specifically increases IRES-dependent translation of this antiapoptotic factor, thereby providing a survival advantage to the cell (*15*). A 50% increase in XIAP protein levels was evident in wild-type MEFs after this stimulus, whereas no induction was evident in *Dkc1*^{m} cells (Fig. 2A and fig. S3, C and D). We next examined the translation of the p27 mRNA during the G_0/G_1 phase of the cell cycle, which has been shown to be increased through its IRES element (*12*, *13*, *16*). Levels of p27 protein were up-regulated by 55% in wild-type cells but this induction was markedly reduced in *Dkc1*^{m} cells (Fig. 2B and fig. S3, A and B). Therefore, the translation of p27 and XIAP mRNAs in *Dkc1*^{m} MEFs is greatly impaired after specific cellular stimuli that affect endogenous IRES-dependent translation.

We next tested whether *Dkc1*^{m} ribosomes could promote the translation of a reporter mRNA directed by the XIAP and p27 IRES elements. To this end, we used the well-established bicistronic expression system to detect IRES activity (*17*, *18*), in which the first cistron is translated by a cap-dependent initiation mechanism and the second is translated by the preceding IRES element (Fig. 2, C and D). IRES-dependent translation of p27 and XIAP mRNAs has been documented with the use of this bicistronic assay (*11*, *13*, *19*). We confirmed IRES-dependent activity of these mRNAs in the primary cells used in our studies and by employing previously reported mutated IRES sequences (fig. S6). To analyze IRES function, we transfected bicistronic reporter mRNAs in wild-type and *Dkc1*^{m} MEFs and used specific stimuli that favor IRES-dependent translation (Fig. 2, C and D, and figs. S4, A to

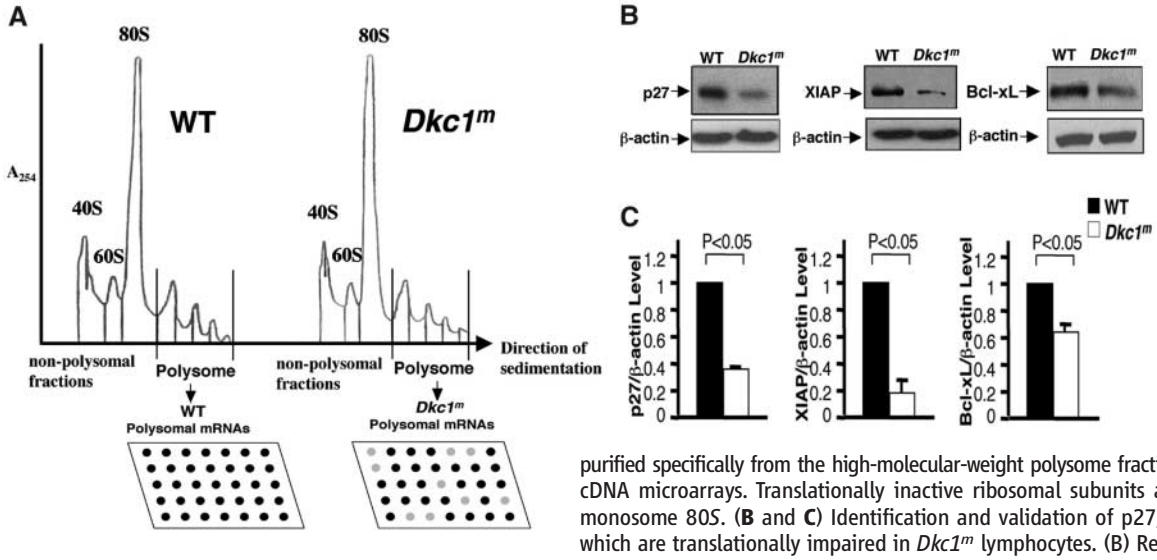

Fig. 1. An unbiased proteomics approach reveals specific translational impairments in *Dkc1*^{m} mice. (**A**) Polyribosomal profiles of wild-type (WT) and *Dkc1*^{m} cytoplasmic extracts from lipopolysaccharide-stimulated primary splenic lymphocytes fractionated on 10 to 50% glycerol gradients. The *y* axis represents the absorbance at 254 nm (A_{254}), and the *x* axis indicates fractions collected. RNA was purified specifically from the high-molecular-weight polysome fractions and used to hybridize cDNA microarrays. Translationally inactive ribosomal subunits are shown: 40*S*, 60*S*, and monosome 80*S*. (**B** and **C**) Identification and validation of p27, XIAP, and Bcl-xL mRNAs, which are translationally impaired in *Dkc1*^{m} lymphocytes. (B) Representative Western blots for p27, XIAP, and Bcl-xL in wild-type and *Dkc1*^{m} lymphocytes. (C) Densitometry analyses of p27, XIAP, and Bcl-xL values normalized against β-actin are shown as graphs. Each value represents the mean ± SD of three independent experiments, and statistical significance is indicated.

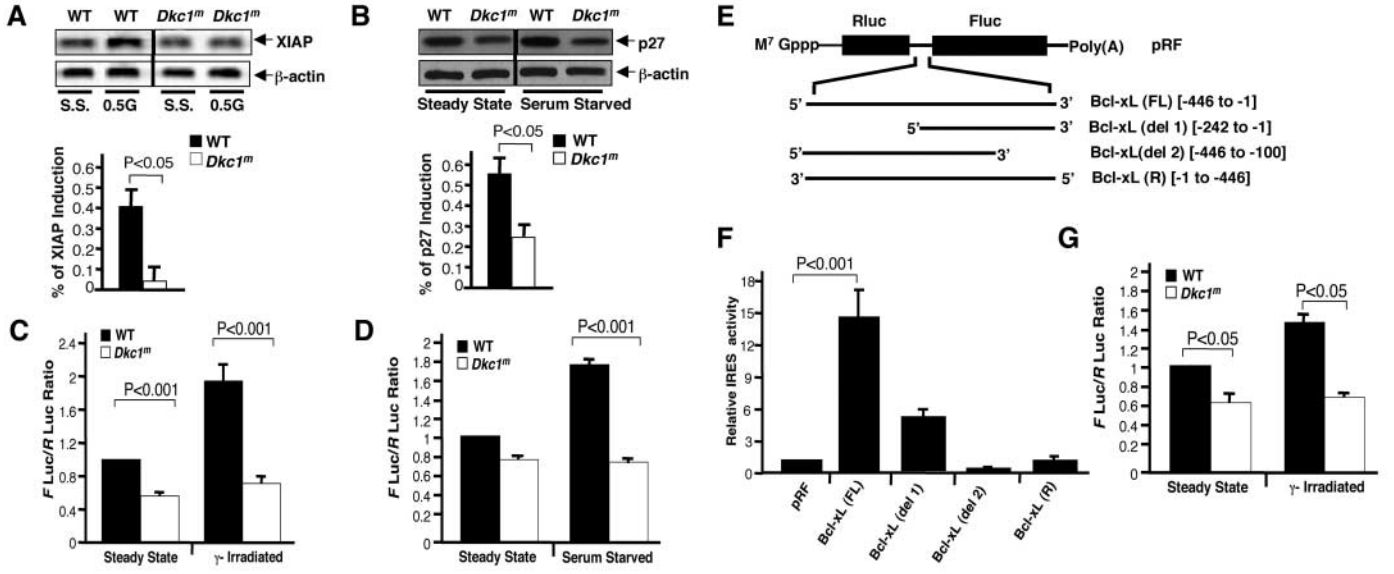

Fig. 2. Impaired IRES-dependent translation of specific cellular mRNAs identified in the proteomics screen in *Dkc1*^{m} mice. (**A**) Representative Western blot of XIAP in the steady state (S.S.) and after γ irradiation (with 0.5 Gy). Induction of XIAP expression (%) is impaired in *Dkc1*^{m} MEFs after γ irradiation. A densitometry analysis after induction (mean ± SEM) from at least three independent experiments is shown. (**B**) Representative Western blot of p27 in the steady state and after serum starvation (in 0.1% fetal bovine serum for 16 hours). Induction of p27 expression (%) is impaired in *Dkc1*^{m} MEFs after serum starvation. A densitometry analysis after induction (mean ± SEM) from at least three independent experiments is shown. (**C**) Wild-type and *Dkc1*^{m} MEFs transfected with the XIAP bicistronic reporter mRNA. The ratio of firefly luciferase to Renilla luciferase (F_{luc}/R_{luc}) (IRES/cap) activity was analyzed in the steady state or after γ irradiation (with 0.5 Gy). Each value is relative to the wild-type F_{luc}/R_{luc} ratio in the steady state, which was set to 1 and represents the mean ± SD of three independent experiments performed in triplicate. Statistical significance is indicated. (**D**) Wild-type and *Dkc1*^{m} MEFs transfected with the p27 bicistronic reporter mRNA. The ratio of F_{luc}/R_{luc} activity was analyzed in the steady state or after serum starvation. Each value is relative to the wild-type F_{luc}/R_{luc} ratio in the steady state, which was set to 1 and represents the mean ± SD of three independent experiments performed in triplicate. (**E**) Schematic diagram of the full-length (FL) Bcl-xL 5′ UTR in the reverse orientation (R) and two deletions (del 1 and del 2) used in bicistronic assays. M^{7} Gppp, 7-Methylguanasine; pRF, bicistronic reporter plasmid. (**F**) MEFs were transfected with the indicated plasmids. The F_{luc}/R_{luc} ratio was calculated, and the expression of the pRF empty vector was set as 1. Each value represents the mean ± SD of three independent experiments in triplicate. IRES-dependent translation is still retained when only 250 nucleotides of the 5′ UTR are used (Bcl-xL del1), but its activity is 35% that of the full-length UTR. The Bcl-xL (del 2) mutant indicates that an important functional domain resides with the first 100 nucleotides of the Bcl-xL IRES. (**G**) Wild-type and *Dkc1*^{m} MEFs transfected with the Bcl-xL bicistronic reporter mRNA. The ratio of F_{luc}/R_{luc} activity was analyzed in the steady state or after γ irradiation (with 0.5 Gy). Each value is relative to the wild-type F_{luc}/R_{luc} ratio in the steady state, which was set to 1 and represents the mean ± SD of three independent experiments performed in triplicate.

D and S5, A and B). At first, we confirmed that both wild-type and *Dkc1*^{m} cells responded equally to these stress stimuli (fig. S4). IRES-dependent translation of XIAP and p27 was specifically affected in *Dkc1*^{m} cells, and IRES-mediated translational induction of these mRNAs by γ irradiation and serum starvation was reduced (Fig. 2, C and D). Therefore, the translation impairment of XIAP and p27 mRNAs in *Dkc1*^{m} cells is at the level of IRES-dependent translation.

Because Bcl-xL was the third mRNA identified in our proteomics screen, we next determined the molecular mechanisms for its translational impairment in *Dkc1*^{m} cells (Fig. 1B). Although Bcl-xL had not previously been reported to contain an IRES element, we tested whether the Bcl-xL 5′ untranslated region (UTR) possesses IRES activity when cloned in a bicistronic vector. These experiments revealed that Bcl-xL contained a functional IRES that could direct the translation of a second cistron and that IRES-dependent translation was abolished when the Bcl-xL 5′ UTR was cloned in a reverse orientation or when deletion mutants were used (Fig. 2, E and F). These findings indicated that a functional IRES element is present –446 to –1 nucleotides upstream of the initiation codon and that IRES-dependent translation is still retained when only 250 nucleotides of the 5′ UTR are used (Bcl-xL del1), but its activity is 35% that of the full-length UTR. We ruled out the presence of cryptic promoters in the Bcl-xL 5′ UTR sequence because RNA transfection of the bicistronic vector retains IRES activity (Fig. 2G), and we confirmed the integrity of the transfected vectors (fig. S5, D and E). Thus, the unbiased proteomics approach identified a cellular mRNA harboring an IRES element in its 5′ UTR, affected in *Dkc1*^{m} cells. We confirmed that the defect in Bcl-xL translation was at the level of IRES-dependent translation, because Bcl-xL IRES activity in bicistronic assays was impaired in *Dkc1*^{m} cells as compared to wild-type cells (Fig. 2G). Moreover, the ratio of Bcl-xL IRES/cap activity was increased after γ irradiation in wild-type cells, whereas this was reduced in *Dkc1*^{m} cells. Taken together, these data demonstrate that *Dkc1*^{m} cells are impaired in promoting the translation of a subset of mRNAs that share a common mode of translation initiation, directed by an IRES element.

To determine the relative contribution of impaired IRES-dependent translation to X-DC pathogenesis, we undertook a direct genetic approach with one of the target mRNAs affected in *Dkc1*^{m} cells. The tumor suppressor p27 is a Cdk inhibitory protein that coordinates accurate cell-cycle progression. Haploinsufficiency in p27 expression results in susceptibility to cancer, and *p27*$^{+/-}$ mice are tumor-prone upon oncogenic challenge, without biallelic inactivation due to loss of heterozygosity (*20*, *21*). We reasoned that reduced p27 translation in *Dkc1*^{m} mice might contribute to the tumor-prone phenotype of these animals (*6*). We therefore tested for a genetic interaction between *Dkc1* and *p27* and focused our analysis on the cell-cycle status of thymocytes, the predominant cell type that shows increased proliferation in *p27*$^{-/-}$ mice (*22*–*24*). Neither *p27*$^{+/-}$ nor *Dkc1*^{m} thymocytes showed differences in cell proliferation as compared to wild-type mice. Thymocytes from *Dkc1*^{m};*p27*$^{+/-}$ mice displayed a marked increase in S phase progression, similar

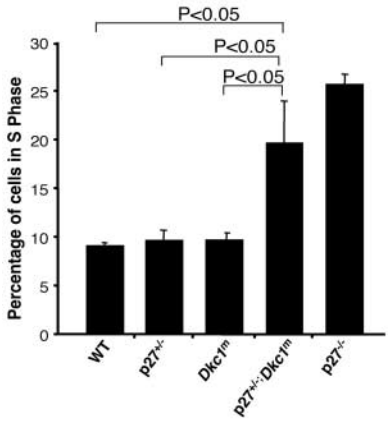

Fig. 3. *Dkc1* cooperates genetically with p27 in cell-cycle control. The cell cycle of thymocytes from indicated genotypes (8 weeks old) was analyzed by flow cytometry after propidium iodide staining. Each bar represents the mean ± SD from six mice. *P* values are indicated.

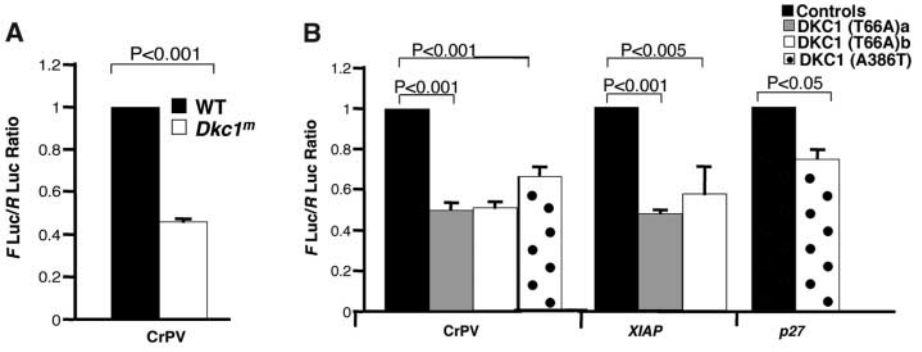

Fig. 4. Molecular role of dyskerin in IRES-dependent translation in X-DC. (**A**) Wild-type and *Dkc1m* MEFs transfected with CrPV bicistronic vector in mRNA form. Each value is relative to the wild-type F_{luc}/R_{luc} ratio, which was set to 1 and represents the mean ± SD of three independent experiments performed in triplicate. (**B**) Human X-DC B-lymphoblast and fibroblast cell lines electroporated with the bicistronic vector mRNAs as indicated. Each value is relative to the control steady state, which was set to 1 and represents the mean ± SD of three independent experiments performed in triplicate. Statistical significance is indicated. The lymphoblast cells lines were derived from two affected brothers with X-DC [DKC1 (T66A)a (DKC1a) and DKC1 (T66A)b (DKC1b)]. As controls, both a normal lymphoblast cell line derived from the unaffected carrier mother as well as two other normal lymphoblast cell lines were used (*7*). The *DKC1* mutant fibroblast cell line [DKC1 (A386T)] was, in turn, compared to three normal human fibroblast lines. All normal and/or carrier cell lines indicated as controls displayed similar values of F_{luc} IRES-mediated translation, which were averaged and set to 1. Each value represents the mean ± SD of three independent experiments performed in triplicate.

to p27$^{-/-}$ cells (Fig. 3). Thus, these findings suggest that reductions in p27 IRES-dependent translation may render *Dkc1m* mice tumor-prone, which is consistent with the cancer susceptibility phenotype manifested in X-DC pathogenesis.

To gain additional insight into the molecular mechanisms by which reductions in rRNA modifications affect IRES-dependent translation, we next investigated whether *Dkc1m* ribosomes are intrinsically impaired in their ability to translate IRES-dependent viral mRNAs via an IRES-dependent mechanism. Many viruses do not possess capped mRNAs and require IRES elements to promote translation initiation. Moreover, the translation of certain viral mRNAs occurs independently of some or all eukaryotic initiation factors (eIFs) of translation employed in cap-dependent translation (*14*). For example, the cricket paralysis virus (CrPV) IRES directly recruits the ribosome on an initiation codon without any canonical eIFs (*25*). It has previously been shown that CrPV IRES is active in mammalian cells, and we confirmed those findings in the primary cells used in our studies and by employing previously published CrPV IRES mutants (*25*–*27*) (fig. S6). To test whether the defect in IRES-dependent translation in *Dkc1m* cells resides in the ribosome, we used the CrPV IRES as a molecular tool. To this end, we transfected a bicistronic reporter mRNA in which the translation of F_{luc} is driven by the CrPV IRES element (Fig. 4A and fig. S5C). The translation of the CrPV IRES was severely impaired in *Dkc1m* cells (Fig. 4A), strongly suggesting that impairments in IRES-dependent translation in *Dkc1m* cells are attributable to an intrinsic defect in *Dkc1m* ribosomes.

We further investigated whether point mutations in the *DKC1* gene, present in X-DC patients, would result in the same translational defects as in hypomorphic *Dkc1m* mice. At first, we analyzed the efficiency of CrPV IRES translation, which relies solely on ribosomal subunits to initiate translation in human X-DC lymphoblasts and fibroblast cell lines (*7*). We observed a specific decrease in CrPV IRES activity in human X-DC patient cells as compared to normal controls (Fig. 4B). We next tested whether translational impairments of particular cellular IRES mRNAs, identified in our proteomics screen, were also evident in X-DC patient cells. A marked decrease in XIAP and p27 IRES-dependent translation was evident (Fig. 4B). Therefore, human X-DC patient cells show a specific defect in IRES-dependent translation. Moreover, mRNAs identified by an unbiased proteomics protocol in *Dkc1m* cells also show a translational impairment in X-DC human cells, thereby representing the first target genes for X-DC pathogenesis.

The full inactivation of *Dkc1* results in a lethal phenotype in yeast, fly, and mouse, supporting the notion that the complete loss of pseudouridine modifications in rRNA may not be compatible with life (*2*). How then could reductions in the activity of a housekeeping gene required for ribosome modification lead to a complex phenotype associated with X-DC disease? In this study, we addressed this question using an unbiased proteomics approach to uncover translational defects in primary cells derived from hypomorphic *Dkc1m* mice, which faithfully recapitulate X-DC pathogenesis (*6*). Our findings indicate that the activity of IRES elements, which regulate the translation of a subset of mRNAs, is affected in *Dkc1m* cells and X-DC human patient cells, thereby providing a molecular mechanism through which decreased rRNA modifications may result in specific phenotypic consequences. In this respect, our proteomics screen has identified two important cellular mRNAs previously shown to possess an IRES element: the tumor suppressor p27 and the antiapoptotic factor XIAP, which are translationally impaired in *Dkc1m* mice and X-DC human patient cells. In addition, this screen led to the unbiased identification of a previously uncharacterized IRES element present in the antiapoptotic factor Bcl-xL, and IRES-dependent translation of this mRNA was defective in *Dkc1m* cells. The deregulated IRES-dependent translation of mRNAs identified in our screen may account for two specific pathological features of X-DC: susceptibility to cancer and bone marrow failure. Because decreases in p27 protein expression are sufficient to result in tumor susceptibility (*20*), reductions in p27 IRES-dependent translation in *Dkc1m* mice and X-DC patient samples is likely to account, at least in part, for the cancer susceptibility phenotype present in X-DC. To this end, we have demonstrated a genetic interaction between *Dkc1* and p27 required for restricted cell-cycle progression. In addition, bone marrow failure, a hallmark of X-DC pathogenesis, is characterized by increased apoptosis of hematopoietic progenitors and stem cells (*28*). Many antiapoptotic factors possess an IRES element in their 5′ UTRs, which promotes translation during stress conditions, thereby providing a survival advantage to the cell (*15*). Therefore, it is tempting to speculate that a combinatorial defect in IRES translation of antiapoptotic factors such as XIAP and Bcl-xL may underlie the bone marrow phenotype in X-DC. Bcl-xL chimeric embryos display increased cell death of hematopoitic progenitors associated with anemia and lymphopenia (*29*, *30*), which are hallmarks of X-DC pathogenesis.

The fact that translation initiation directed from CrPV IRES, which relies solely on the ribosome itself, is severely impaired in *Dkc1*^{m} cells strongly implies that the molecular defect intrinsically resides in the inability of *Dkc1*^{m} ribosomes to efficiently engage the IRES element. Taken together, these findings allow us to propose a model whereby reductions in rRNA modifications due to dyskerin malfunction affect the translation of important cellular IRES mRNAs, which may require more direct interactions with the ribosome for translation initiation, thereby contributing to specific pathological features of X-DC. Although we cannot determine how defects in other cellular functions attributed to dyskerin activity may contribute to X-DC, these findings indicate a previously unknown molecular mechanism by which impairments in rRNA modifications affect translation control and lead to disease pathogenesis.

References and Notes

1. I. Dokal, *Br. J. Haematol.* **110**, 768 (2000).
2. U. T. Meier, *Chromosoma* **114**, 1 (2005).
3. J. Ni, A. L. Tien, M. J. Fournier, *Cell* **89**, 565 (1997).
4. C. Wang, C. C. Query, U. T. Meier, *Mol. Cell. Biol.* **22**, 8457 (2002).
5. Y. Mochizuki, J. He, S. Kulkarni, M. Bessler, P. J. Mason, *Proc. Natl. Acad. Sci. U.S.A.* **101**, 10756 (2004).
6. D. Ruggero *et al.*, *Science* **299**, 259 (2003).
7. Materials and methods are available as supporting material on *Science* Online.
8. N. A. Gasper, C. C. Petty, L. W. Schrum, I. Marriott, K. L. Bost, *Infect. Immun.* **70**, 4075 (2002).
9. V. Sharma, M. Delgado, D. Ganea, *J. Immunol.* **176**, 97 (2006).
10. A. J. Stauber *et al.*, *Mol. Pharmacol.* **67**, 681 (2005).
11. M. Holcik, C. Lefebvre, C. Yeh, T. Chow, R. G. Korneluk, *Nat. Cell Biol.* **1**, 190 (1999).
12. W. K. Miskimins, G. Wang, M. Hawkinson, R. Miskimins, *Mol. Cell. Biol.* **21**, 4960 (2001).
13. M. Kullmann, U. Gopfert, B. Siewe, L. Hengst, *Genes Dev.* **16**, 3087 (2002).
14. C. U. Hellen, P. Sarnow, *Genes Dev.* **15**, 1593 (2001).
15. M. Holcik, N. Sonenberg, *Nat. Rev. Mol. Cell Biol.* **6**, 318 (2005).
16. S. S. Millard *et al.*, *J. Biol. Chem.* **272**, 7093 (1997).
17. J. Pelletier, N. Sonenberg, *J. Virol.* **63**, 441 (1989).
18. M. Stoneley, F. E. Paulin, J. P. Le Quesne, S. A. Chappell, A. E. Willis, *Oncogene* **16**, 423 (1998).
19. S. Cho, J. H. Kim, S. H. Back, S. K. Jang, *Mol. Cell. Biol.* **25**, 1283 (2005).
20. M. L. Fero, E. Randel, K. E. Gurley, J. M. Roberts, C. J. Kemp, *Nature* **396**, 177 (1998).
21. J. Philipp-Staheli, S. R. Payne, C. J. Kemp, *Exp. Cell Res.* **264**, 148 (2001).
22. M. L. Fero *et al.*, *Cell* **85**, 733 (1996).
23. H. Kiyokawa *et al.*, *Cell* **85**, 721 (1996).
24. K. Nakayama *et al.*, *Cell* **85**, 707 (1996).
25. J. E. Wilson, T. V. Pestova, C. U. Hellen, P. Sarnow, *Cell* **102**, 511 (2000).
26. E. Jan, P. Sarnow, *J. Mol. Biol.* **324**, 889 (2002).
27. C. P. Petersen, M. E. Bordeleau, J. Pelletier, P. A. Sharp, *Mol. Cell* **21**, 533 (2006).
28. I. Dokal, *Curr. Opin. Hematol.* **3**, 453 (1996).
29. N. Motoyama *et al.*, *Science* **267**, 1506 (1995).
30. M. Socolovsky, A. E. Fallon, S. Wang, C. Brugnara, H. F. Lodish, *Cell* **98**, 181 (1999).

31. We are indebted to M. Barna for helpful discussions and critical reading of the manuscript. We thank A. Koff for the p27$^{-/-}$ mice; M. Holcik, L. Hengst, and P. Sarnow for reagents; K. Zaret, J. Burch, E. Golemis, and J. Testa for critical reading of the manuscript; and FCCC core facilities and J. Grant for technical assistance.

Supporting Online Material

www.sciencemag.org/cgi/content/full/312/5775/902/DC1
Materials and Methods
Figs. S1 to S6

14 December 2005; accepted 13 April 2006
10.1126/science.1123835

RNA Recognition and Cleavage by a Splicing Endonuclease

Song Xue, Kate Calvin, Hong Li*

The RNA splicing endonuclease cleaves two phosphodiester bonds within folded precursor RNAs during intron removal, producing the functional RNAs required for protein synthesis. Here we describe at a resolution of 2.85 angstroms the structure of a splicing endonuclease from *Archaeglobus fulgidus* bound with a bulge-helix-bulge RNA containing a noncleaved and a cleaved splice site. The endonuclease dimer cooperatively recognized a flipped-out bulge base and stabilizes sharply bent bulge backbones that are poised for an in-line RNA cleavage reaction. Cooperativity arises because an arginine pair from one catalytic domain sandwiches a nucleobase within the bulge cleaved by the other catalytic domain.

The removal of intervening sequences in functional RNAs is required in all domains of life. Introns found in nuclear tRNA and archaeal RNA are removed by protein enzymes—an endonuclease, a ligase, and, in some organisms, a 2′-phosphotransferase (*1*–*5*).

Critical to this splicing mechanism are the recognition of the intron-exon junctions and the subsequent breakage of the two phosphodiester bonds. This process is mediated by the endonuclease. The splicing endonucleases characterized so far belong to one of four families: homodimers (α_2) (*6*), homotetramers (α_4) (*7*), homodimers of two heterodimers ($\alpha_2\beta_2$) (*8*, *9*), or heterotetramers ($\alpha\beta\delta\gamma$) (*10*–*12*). Despite the differences in subunit composition, all splicing endonucleases comprise two conserved catalytic units and two structural units that play roles in correctly orienting the catalytic sites (*13*).

All splicing endonucleases recognize the bulge-helix-bulge (BHB) motif that is composed of two three-nucleotide bulges separated by 4 base pairs (bp) (*6*, *8*, *9*, *14*–*16*). Each bulge contains a cleavage site immediately after the second bulge nucleotide. In addition to the recognition of the canonical BHB RNA motif, splicing endonucleases of different families exhibit distinct substrate recognition properties. The localized structural fold of the BHB motif is sufficient for the removal of archaeal introns from various segments of precursor transfer RNA (tRNA), ribosomal RNA (rRNA), and some mRNA; the secondary structure of the BHB motif is solely responsible for its recognition by the archaeal splicing endonuclease (*17*–*20*). Nuclear precursor tRNAs, however, have additional recognition elements in their mature domains that are required for splicing (*16*, *21*–*23*). The eukaryal $\alpha\beta\delta\gamma$ splicing endonuclease is composed of Sen2, Sen34, Sen54, and Sen15 subunits and locates the splice sites via a "ruler mechanism." This mechanism requires the specific recognition of two features in precursor tRNAs: the cloverleaf structure of the mature domain (*21*, *24*) and an anticodon-intron base pair (A-I pair) adjacent to the 3′ bulge (*22*, *23*). It has been proposed that the eukaryal endonuclease, while maintaining the ability to recognize the minimal BHB RNA, has acquired additional RNA recognition properties.

Based on the cleavage products and conserved catalytic residues, all splicing endonucleases appear to use a similar mechanism. Cleavage by the splicing endonuclease generates 5′-hydroxyl and 2′,3′-cyclic phosphate termini (*1*, *2*, *25*). These products suggest an S_N2-type in-line attack by the nearby 2′-hydroxyl on phosphorus and a trigonal bipyramidal transition state, similar to that used by the RNase A family of ribonucleases (*26*). In previously determined archaeal-splicing endonuclease structures, three invariant residues—a histidine, a lysine, and a tyrosine—form a closely spaced triad. In the *Methanococcus jannaschii* endonuclease structure, a bound sulfate ion, which was proposed to mimic a phosphate, was found in the center of the triad (*27*), which further implicates the triad in RNA cleavage. However, there is no structural evidence to confirm the catalytic roles of each of the triad residues, and the catalytic mechanism of the splicing endonuclease remains elusive.

We have determined the cocrystal structure of a dimeric splicing endonuclease from *Archaeglobus fulgidus* (AF) bound to a BHB RNA that was formed from two annealed 21-oligomer synthetic oligonucleotide (see Fig. 1A). One strand of the RNA contains a 2′-deoxy–

Department of Chemistry and Biochemistry, Institute of Molecular Biophysics, Florida State University, Tallahassee, FL 32306, USA.

*To whom correspondence should be addressed. E-mail: hongli@sb.fsu.edu

ERRATUM

Post date 1 September 2006

Reports: "Impaired control of IRES-mediated translation in X-linked dyskeratosis congenita" by A. Yoon *et al.* (12 May 2006, p. 902). The third author's name was spelled incorrectly; it should be Yves Brandenburger.